DOI:10.1021/jf100665u

JOURNAL OF AGRICULTURAL AND FOOD CHEMISTRY
ARTICLE

Laser-Induced Breakdown Spectroscopy and Chemometrics: A Novel Potential Method to Analyze Wheat Grains

Milena R. Martelli,[†] François Brygo,[‡] Abdelkrim Sadoudi,[†] Philippe Delaporte,[‡] and Cécile Barron*,[†]

[†]INRA, UMR 1208 "Ingénierie des Agropolymères et Technologies Emergentes", INRA-CIRAD-UMII-Supagro, F-34000 Montpellier, France, and [‡]CNRS, UMR 6182 "Laboratoire Lasers, Plasmas et Procédés Photoniques", CNRS-Université de la Méditerranée, 13288 Marseille, France

Laser-induced breakdown spectroscopy (LIBS) has been widely used to evaluate the elemental composition (e.g., minerals or metal accumulation) on vegetal tissues. The main objective of this work was to differentiate wheat outer tissues during the grain ablation using LIBS and univariate/multivariate analysis. A high resolution spectrometer and a Nd:YAG laser (532 nm, 5 ns) was first used in order to easily identify atomic wheat emission lines. Then a pulsed excimer laser ArF (193 nm, 15 ns) and a compact fiber optic spectrometer was used to acquire LIBS spectral data from each pulse. Univariate and multivariate analyses (MW2D, PLS-DA) were carried out to provide more in depth information from the LIBS experiment. The number of pulses needed to ablate wheat tissues was successfully predicted by the supervised pattern recognition procedure. LIBS used in conjunction with multivariate analysis could be an interesting technique for rapid structural analysis of vegetal material.

KEYWORDS: Wheat grain; LIBS; partial least-squares; moving 2D; aleurone; cohesion

INTRODUCTION

Wheat grain is a complex structure made of the germ and starchy endosperm surrounded by several peripheral tissues differing in their structure and chemical compositions (*1*, *2*). They are formed by a multilayer adhered system made up, from the outer to the inner surface, of the pericarp (PE), which is divided into outer (OP) and inner pericarp (IP), then the seed coat (SC), next the nucellar epidermis (NE), and finally the aleurone layer (AL). These tissues are composed mainly of polysaccharides (cellulose, arabinoxylans, mixed-linked β-glucans), proteins, lipids, vitamins, and minerals (*2*). The peripheral tissues are separated from the starchy endosperm, using conventional milling, and recovered in the bran fraction. However, bioactive compounds are mainly concentrated in the bran fractions (micronutrients, antioxidants, and fibers). New milling technologies are being developed in order to fractionate bran into food ingredients or incorporate nutritive outer layers in wheat flour. The mechanical properties of wheat grain outer layers are key properties to explain differences observed during the bran fractionation in the milling processes (*3*, *4*). Up to now, these properties have been measured by tensile tissue tests obtained after hand isolation (*3*−*8*). However, the soaking step required during the sample preparation can modify their physicochemical composition and then their mechanical properties (*8*, *9*). A recent study has shown that wheat outer tissue properties can be revealed by pulsed laser ablation on native grain using an excimer laser ArF (193 nm, 15 ns) (*10*). Tissue ablation rate can be indirectly related to its cohesion because tissue optical properties and laser parameters are the same (*11*). The pulse ablation rates are determined by the material loss during ablation, either using the depth (μm/pulse), the volume (μm^3/pulse), or the material (ng/pulse) losses. Martelli et al. (*10*) have investigated the depth of the spot area by microscopic observation of wheat cross-sections after ablation. The thin outer tissues, from 2 to 70 μm (*12*, *13*), were gradually ablated during 100 pulses and the ablation rate was calculated using image analysis: 0.4 μm/pulse for SC ablation and 1.5 μm/pulse for PE ablation. However, these observations are very time-consuming, limiting the laser application. Thus, LIBS could be a powerful tool to follow wheat tissue ablation in real time by taking advantage of compositional heterogeneity within the peripheral tissues.

LIBS has been demonstrated as a potential technique for qualitative analysis or even quantitative determination of elemental compositions. The detection of soil nutrients (*14*), organic compounds (*15*−*19*), and geological materials (*20*) has been one of the useful LIBS applications. More specifically, micronutrients (Cu, Mn, Fe, and Zn) or macronutrients (P, K, Ca, Mg) were detected in plant materials (*21*, *22*). LIBS required no sample preparation and could be carried out in situ in a limited time. LIBS technique could be then used to determine spatial distribution of interesting elements such as toxic elements on vegetal tissues (*23*, *24*). The spectral data of the emission spectrum provide multielement information on the chemical composition of the sample.

In LIBS investigations, the element concentration is traditionally given by univariate analysis. For biological samples, the success of the LIBS application involves the development and optimization of statistical methods to interpret their complex

*To whom correspondence should be addressed. Phone: +33 4 99 61 31 04. Fax: +33 4 99 61 30 76. E-mail: barron@supagro.inra.fr.

 Published on Web 05/26/2010

signatures with subtle differences. Recently, multivariate data analyses have been applied on LIBS spectra (*16*, *25*−*29*) in order to better exploit its complex information.

Chemometrics offers helpful tools to process huge spectral data (made up of more than 2000 variables) and is widely used in vibrational spectroscopy (near infrared, Raman). These statistics-based methods considered the whole spectral intensities to explore the variability within the data set in order to classify or quantify samples (*30*, *31*). They can be unsupervised procedures, i.e., without prior knowledge of the existence of classes, like principal component analysis (PCA), two-dimensional (2D), and moving window 2D (MW2D) correlation, or supervised procedures, i.e., those methods incorporating prior knowledge of class identity, like the pattern recognition technique (partial least squares−discriminant analysis, PLS-DA).

Unsupervised methods are a good starting point to discriminate and interpret data before class elaboration. PCA is the most commonly used discriminant analysis tool for high-dimensional data, however it is only capable of identifying large variability and it is not capable of distinguishing "among-groups" and "within-groups" variability (*32*). MW2D uses the generalized 2D correlation to represent spectral intensity variations along a variable perturbation (mainly time or temperature) (*33*). Supervised classification techniques, such as PLS-DA, need a first step of training assuming the data structure before being able to predict which class it belongs to. A multivariate model that separates classes of observations on the basis of the spectral data is then built. Hence chemometry could be a powerful tool to extract information from a large collection of LIBS spectra collected from each pulse during a multilayer material ablation.

In this study, LIBS experiment and univariate/multivariate analyses were used with the aim to differentiate wheat tissues during the grain gradual ablation in real time, without any sample preparation. First, LIBS spectral signatures of hand-isolated tissues were collected in order to identify specific signals related to each wheat layer chemical composition. Then, spectral changes noted during the multilayer ablation were identified using the MW2D algorithm and univariate analysis. Specific identification of each tissue was further carried out by PLS-DA on all spectral data in order to identify the number of pulses required to ablate each tissue and then determine the ablation rate.

MATERIALS AND METHODS

Sample Preparation. Two cultivars of common wheat (*Triticum aestivum* L.) of different kernel hardness were used in this study: Tiger (hard) and Crousty (soft), harvested in 2005 in Germany and France, respectively. Before LIBS experiments, grains were selected according to their thickness (2.85 ± 0.05 mm) with the aid of a caliper, and then they were conditioned at constant relative humidity (53%) by using a saturated $Mg(NO_3)_2$ solution at 25 °C for at least 1 week until the laser experiments.

Tissues Isolated from Wheat Bran. Tissues were isolated by hand according to radial grain orientations. Germ and brush were cut before grain immersion in distilled water for 12−16 h. Outer tissues were obtained by removing the endosperm using a scalpel. Tissues were separated with a scalpel as described by Barron et al. (*9*): OP, IP, SC, NE, and AL. OP and AL were separated from the Crousty and Tiger cultivars; IP, SC, and NE were separated also from another wheat cultivar (Caphorn, red wheat as the other). Samples were dried between two microscopic slides under ambient conditions to flatten them, and their moisture content (12%) was adjusted by conditioning at constant relative humidity (53%) using a saturated $Mg(NO_3)_2$ solution at 25 °C for at least 1 week until laser experiments.

Laser Induced Breakdown Spectroscopy. The first step of this work was to obtain a global atomic spectrum with a high resolution spectrometer (echelle spectrometer connected to a Nd:YAG laser) in order to identify the emission lines from wheat laser ablation. However, this experimental system was not adapted to follow the ablation of thin tissues due to the high laser energy necessary to obtain an interpretable signal. Since a previous work (*10*) showed that an excimer laser ArF 193 nm was successfully used to gradually ablate wheat outer tissues on native grains, the same experimental set up was then connected to a miniature fiber optic spectrometer. First, LIBS spectra were acquired from each pure tissue in order to better interpret the data collected during the native grain ablation.

Pulsed Laser Ablation with an Nd:YAG Laser. Wheat grains were ablated with a Q-switched Nd:YAG laser (Brio, Quantel) operating in its second harmonic wavelength at 532 nm. The pulse duration was 5 ns and the repetition rate was 20 Hz. The energy per pulse was 80 mJ, with a circular surface of 120 μm diameter at the focal point. An optical fiber (UV/Vis, 1000 μm core diameter, 2 m length) collected the emission at the entrance of an Aryelle Butterfly spectrometer (Laser Technik Berlin, LTB, Germany, $\lambda/\Delta\lambda = 10000$), and the spectra were recorded with a pulsed intensified CCD camera (iStar, Andor). In each measurement, the plasma emissions of 10 laser pulses were averaged.

Pulsed Laser Ablation with an ArF Laser. Wheat grains and tissues were ablated with an argon fluoride (ArF) LPX 220i (Lambda Physics, Germany) operating at 193 nm with a pulse duration of 15 ns and a repetition rate of 1 Hz. A spectrometer HR2000 (Ocean Optics, USA) was connected to the laser experimental set up by an external trigger. The laser beam went through a metallic mask to keep a uniform part of the beam. Then a spherical lens was used to image the mask plane with the required reduction on the sample to obtain a near-uniform irradiation of the grain. Laser fluence or spatial energy density (energy per unit area) was 2 J cm^{-2}. Plasma light was directly collected through an optical fiber VIS/NIR (1000 μm core diameter, 2 m length) for isolated layers (OP, IN, SC, NE, and AL) and UV/Vis (600 μm core diameter, 2 m length) for composite layers and grains. The angle of collection did not change for sample analysis. The end of the optical fiber was connected to the entrance slit of the spectrometer. An external trigger was used to control the single shot mode. The detector has a gated CCD camera having 14 μm × 200 μm pixels size on a large wavelength range (200−1100 nm). The spectral resolution was 1 nm with an integration time of 2 ms. The sample holder was fixed on long-range motorized translation stage that permitted a precise repositioning of the irradiated zone under an optical microscope (Olympus, BXFM) in conjunction with a digital camera (Qimaging QICAM, Fast 1394) and then the observation of the ablation surface between laser pulses. Isolated tissue was analyzed only once due to the difficulty of sample preparation. Thirteen to fifteen wheat grains were analyzed from each cultivar. LIBS analyses were performed in air under atmospheric pressure.

Spectral Statistical Treatments. *Spectra Pretreatment*. Before statistical analysis, spectral data were baseline corrected and normalized according to the intensity of the C_2 Swan Molecular Band (516.52 nm) to compensate for any experimental fluctuations or laser−matter interactions (plasma temperature, crater depth, and tissue density). Mineral contents could not be used due to the differences in tissue composition (*34*). Because the aim of this study was to discriminate wheat tissues and not to quantify element contents, C_2 was the most convenient choice for the normalization, taking into account their homogeneous distribution on biological tissues (*18*, *34*).

Moving-Window Two-Dimensional (MW2D) Correlation. Moving-window two-dimensional (MW2D) correlation was carried out on a data matrix containing all spectral intensities ordered with respect to pulse number (from 1 to 120 pulses), by using the 2Dshige software (*35*). The spectral intensities from each individual spectrum were mean-centered. MW2D was performed as follows: (1) subdivision of the entire data matrix chosen selectively by a moving window with an arbitrarily fixed window size, (2) calculating an autocorrelation for each subset of the data, (3) plotting the autocorrelation thus obtained as a function of the local average value of the perturbation variable within the window. MW2D autocorrelation analysis was applied to the spectral data obtained by LIBS and normalized according to the total spectral area with the number of pulses as the perturbation variable. Window size was changed from 7, 13, 17, and 25. The number of 13 spectra was defined as being the optimum number of spectra necessary to obtain a MW2D with low noise and high peak resolution. A similar autocorrelation analysis was then applied on this new window. The window was moved step by step until all of the spectra were included. The 2D maps were then produced by plotting the autocorrelation intensities as a function of the window. Peaks could then

be observed in a 2D plot at the number of pulses where the largest spectral variations occur (*33*).

Partial Least Squares−Discriminant Analysis (*PLS-DA*). Chemometric methods such as partial least squares−discriminant analysis (PLS-DA) is a multivariate inverse least-squares discrimination method used to classify samples. PLS-DA is based on a classical PLS regression, which provides a multivariate linear model for the relationship between a set of prediction variables X, and a set of response variables Y. As in multiple linear regression, the main purpose of PLS is to build a linear model:

$$Y = XB + E \quad (1)$$

where Y is an $n \times p$ variables response matrix, X is an $n \times m$ variables predictor matrix, B is a $m \times p$ matrix of scores, and E is an error matrix for the model which has the same dimensions as Y. Spectral data (X) are highly correlated, so the first step of PLS is to transform input variables into latent variables (LVs) in order to minimize the error. In the case of PLS-DA, the response variable is expressed by class membership. A Y-block is created with a variable for each class, where 1 indicates a sample belongs to a class, and 0 indicates that it does not. Then the PLS predicts the class number for each sample where the rotation of the LVs is focused on class separation. The PLS-DA analysis provides the percentage of correct classification and the loadings of each species on each LV. This analysis expressed also the statistical parameters indicating the modeling efficiency given by parameters of sensitivity and specificity. The sensitivity is the percentage of the samples of a category accepted by the class model. The specificity is the percentage of the samples of the categories which are different from the modeled one, rejected by the class model. Then the PLS-DA was calculated. All data processing and modeling were performed in MatLab 7.0 (The Mathworks Inc.) using the PLS Toolbox 3.5 (Eigenvector Research Inc.). Calibration data set was about 25 spectra per tissue per cultivar. Validation was made by two methods: (i) a cross-validation (venetian blinds) using the calibration data set, and (ii) an external validation using test data set using eight or nine spectra per tissue per cultivar.

Confocal Scanning Laser Microscopy (CSLM). Grains were humidified for 16 h at 4 °C and fixed in 20 mL L^{-1} gluteraldehyde in 0.1 mol L^{-1} phosphate buffer (pH 7.0) for 4 h at 20 °C, washed in water five times for 10 min. Cross-sections, 60 μm thick, were cut with a vibratome (Microcut H1200) and stained with Nile Red (Nile Blue A Oxazone) and Calcofluor White M2R (Fluorescent Brightener 28), counterstained by Fast Green (*36*) as described by Martelli et al. (*10*). Stains were purchased from Sigma-Aldrich Co. (USA). Sections were observed using a Zeiss confocal laser scanning microscope LSM510 AX70 (Carl Zeiss, Germany) in the Montpellier Rio Imaging (MRI) facility. Calcofluor was excited at 405 nm, and light emitted was recorded between 420 and 480 nm by a band-pass filter. Nile Red was excited at 488 nm and emission wavelengths were found to be higher than 560 nm.

RESULTS AND DISCUSSION

Reference LIBS Spectra. *LIBS Signature from Wheat Grain.* Wheat outer layers are mainly composed of carbohydrates (65−79%) but also contain significant amounts of protein (8−19%), lipids (1−3%), and water (8−15%) as well as vitamins (thiamine, riboflavin, niacin, and pyridoxine) and minerals (*2*). Wheat grain LIBS spectrum acquired using a Q-switched Nd:YAG laser connected to a high-resolution spectrometer showed that emission lines came from molecular structures (CN, C_2), organic element (C), as well as some mineral elements: Fe, Mg, Mn, Ca, K, Na, and P (*37*) (**Figure 1**).

LIBS emission lines intensities could depend not only on the concentration of the sample compounds but also on the interaction between the laser-induced plasma and the atmospheric air. Even if LIBS experiments under argon atmosphere could minimize the atmospheric air contribution on interesting emission lines C, C_2, and CN (*29*), the main objective of this work was not to quantify analytical emissions, but identify the differences encountered during wheat ablation.

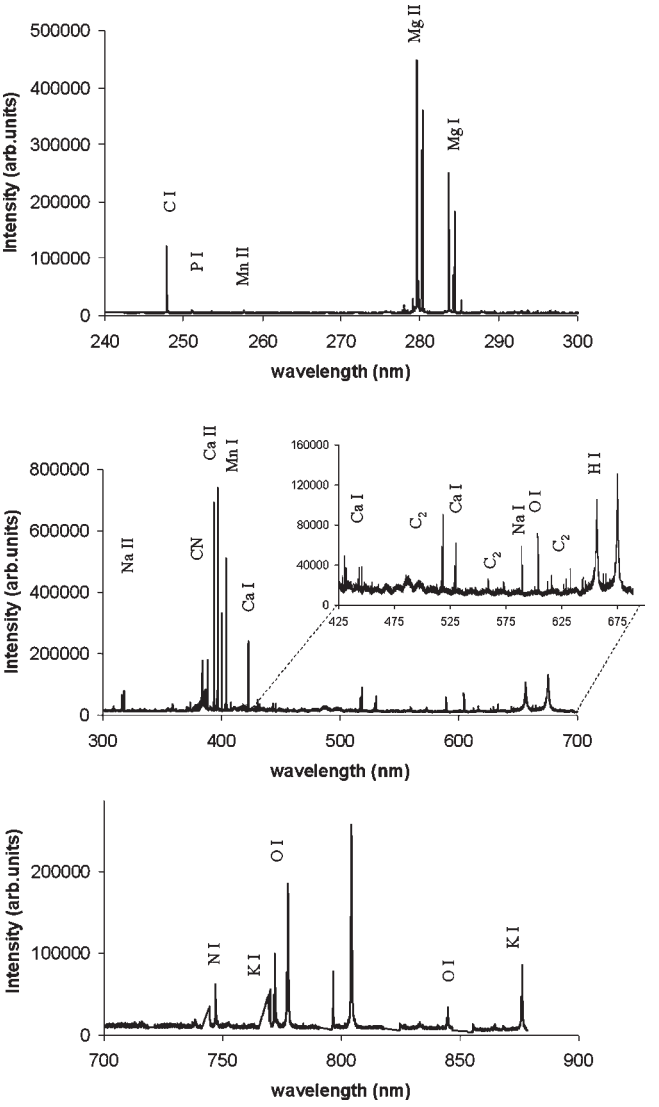

Figure 1. LIBS spectrum obtained for wheat grain (Crousty) with the delay of 500 ns with respect to the laser pulse using an Nd:YAG laser. Laser pulse energy was 80 mJ. The spectra were averaged with 10 pulses.

Some authors showed that the occurrence of C_2 could be derived from the presence of molecules with aromatic rings (multiple C−C bonds) (*19*), such as lipids in the AL and SC tissues, polysaccharides (starch or cell wall polymers). In wheat, dicarbon molecules could be also present in the connection of carboxyl group −COOH to carbon atoms in phenolic compounds or amino acids. The CN molecular bands may be originated from the connection of amino group (NH_2 or NH) to carbon atoms in amino acids (*18*), not discarding the remote possibility of air−plasma interactions (C_2 and atmospheric nitrogen) (*19*). The same observation was made for organic elements (C I 247.86 nm, O I 777 nm, H I 656.28 nm, and N I 746.83 nm), of which one part came from atmospheric air interactions rather than from the basic components of the whole grain.

Mineral elements detected in LIBS spectrum are known to be present in wheat grains, in particular in the AL, with a concentration of about 60% of the total minerals in the kernel (*2*). With regard to the analyses carried out on specific tissues (*2*, *38*), the plasma mineral elemental emission lines (P, Mg, Na, and Ca) are assigned more specially to the aleurone granules in the AL. Emission lines of iron were also observed to be around 272 and

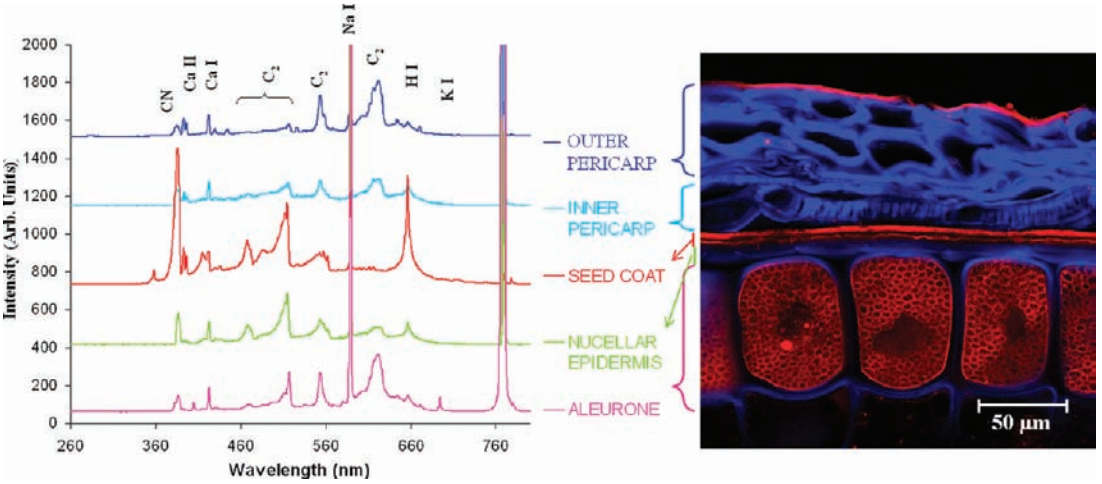

Figure 2. Cross-section of wheat grain outer tissues observed by CSLM with their respective plasma raw spectra obtained by LIBS, using an excimer laser (ArF, 193 nm) and a spectrometer HR 2000.

382 nm. Thus emission lines from minerals could be very practical to discriminate wheat tissues during ablation.

LIBS Signals of Isolated Tissues. Wheat outer tissues are made of superposition of tissues, which are known to have a specific composition. To evaluate if LIBS experiment could indicate differences in tissue composition, reference spectra of pure tissue (hand isolated) were acquired (**Figure 2**).

OP and IP could not be clearly distinguished from their LIBS spectra, as already observed by infrared spectroscopy (*39*), supporting similar composition. In comparison to other tissues, the SC gave the most intense spectrum, but no specific emission lines were observed. Specific mineral emission lines (Mg, P) were expected for AL, however, these elements have intense lines on the UV range and phosphorus lines are more intense after 900 nm. Therefore, a UV/Vis optical fiber was used to evaluate wheat outer tissue ablation on native grains.

Chemical differences were not obvious by direct visual evaluation of the isolated layer spectra. Complexity of the LIBS spectra and wheat tissue composition suggest that interpretation may benefit from the application of multivariate statistical techniques.

Gradual Ablation of Wheat Grain. Atomic LIBS spectra were then acquired from each sequential pulse during wheat grain ablation. Experimental conditions were chosen in order to (i) gradually ablate the wheat grain outer tissues without any thermal effect and (ii) maximize the spectral intensities for all tissues, avoiding the saturated intensities. Gradual ablation was obtained with an ArF pulsed laser and fluence was tested (1, 2, 3, 4, and 5 J cm^{-2}, data not shown) and adapted to have correct spectra for all the tissues. The optical fiber was maintained next to the sample at the same position for these tests. A suitable compromise to obtain interpretable signals was observed using 2 J cm^{-2}.

First, unsupervised exploratory data analysis was carried out using the MW2D in order to detect any changes in emission line intensities during wheat ablation. Once specific spectral regions were identified, univariate analysis of specific lines allowed the qualitative identification of each layer and was confirmed by microscopic observations. Finally, a supervised classification method was performed in order to quantify the number of pulses needed to ablate each tissue.

Exploratory Analysis Using MW2D and Emission Line Intensities. The MW2D method is usually applied to analyze chemical modification as a function of the time or the temperature by vibrational spectroscopy (*33*). In our case, the perturbation axis was the number of pulses during the ablation. The aim was to identify tissue transition from spectral intensity variations without any prejudgment. The MW2D interpretation is based on the fact that intensity variations should be observed at the interface of two tissues. Typical MW2D correlation spectra generated from LIBS spectra during wheat ablation were presented in **Figure 3A** for the spectral ranges 270−290 and 380−430 nm. Almost similar MW2D results were obtained for samples of both cultivars Crousty and Tiger. Four atomic/molecular bands varied according to the pulse number: around 279, 393, 396, and 422 nm, which could be related to the peaks of Mg II (279.55 nm), Ca II (393.37, 396.85 nm), and Ca I (422.67 nm) (*37*), respectively. As shown by Heard et al. (*34*), these minerals are mainly concentrated in the aleurone grains and in the seed coat. In this manner, the spectral intensity transition of 2D correlation spectrum at 396.85 and 279.55 nm was plotted as a function of the pulse number (**Figure 3B**) in order to detect transitions between each tissue. An intense emission line change was observed for Ca II, mainly at 9, 19, and 29 pulses and for Ca I, at 11 and 28 pulses. The magnesium peak (Mg II 279.55 nm) changes was mainly at 36 and 110 pulses and smaller variations around 17 pulses. Univariate analysis confirmed MW2D observations (**Figure 3C**). An increase of peak intensities of Ca II (396.85 nm) was observed between 1 and 9 pulses, and between 19 and 31 pulses, and a constant increase of Mg II (279.55 nm) from 17 to 28 and from 36 to 114 pulses. Martelli et al. (*10*), using similar fluence (2.5 J cm^{-2}), showed that the SC was gradually ablated between 21 and 29 pulses and AL between 33 and 100 pulses. According to mineral distribution in wheat grain (*34*) and the number of pulses to ablate each tissue, both specific peak transitions could occur at tissue transitions. Thus, the transition observed at 17/19 and 28/29 pulses by MW2D (Ca II and Mg I) could be due to the beginning and the ending of SC ablation, respectively, and those at 36 and 110 pulses seem to be due to the AL ablation. The smaller variations at the beginning of wheat ablation at 9 pulses (Ca II) could be due to some differences among OP and IP.

Microscopic observations were carried out on the cross-sections of target grains ablated until Ca II intensity increase (**Figure 4A**,**B**) and decrease (**Figure 4C**) and Mg II increase (**Figure 4D**). Cell walls were stained with Calcofluor, and their fluorescence was then observed in the blue plane, whereas lipids in cuticular layers and aleurone granules were stained with Nile Red and observed in the red plane of the CSLM micrograph. After 20 pulses, the SC was still intact, whereas after 25 pulses, the cuticular layer of SC was no longer always visible (**Figure 4A**,**B**). After 31 pulses, SC was no longer visible, and only a few pieces of

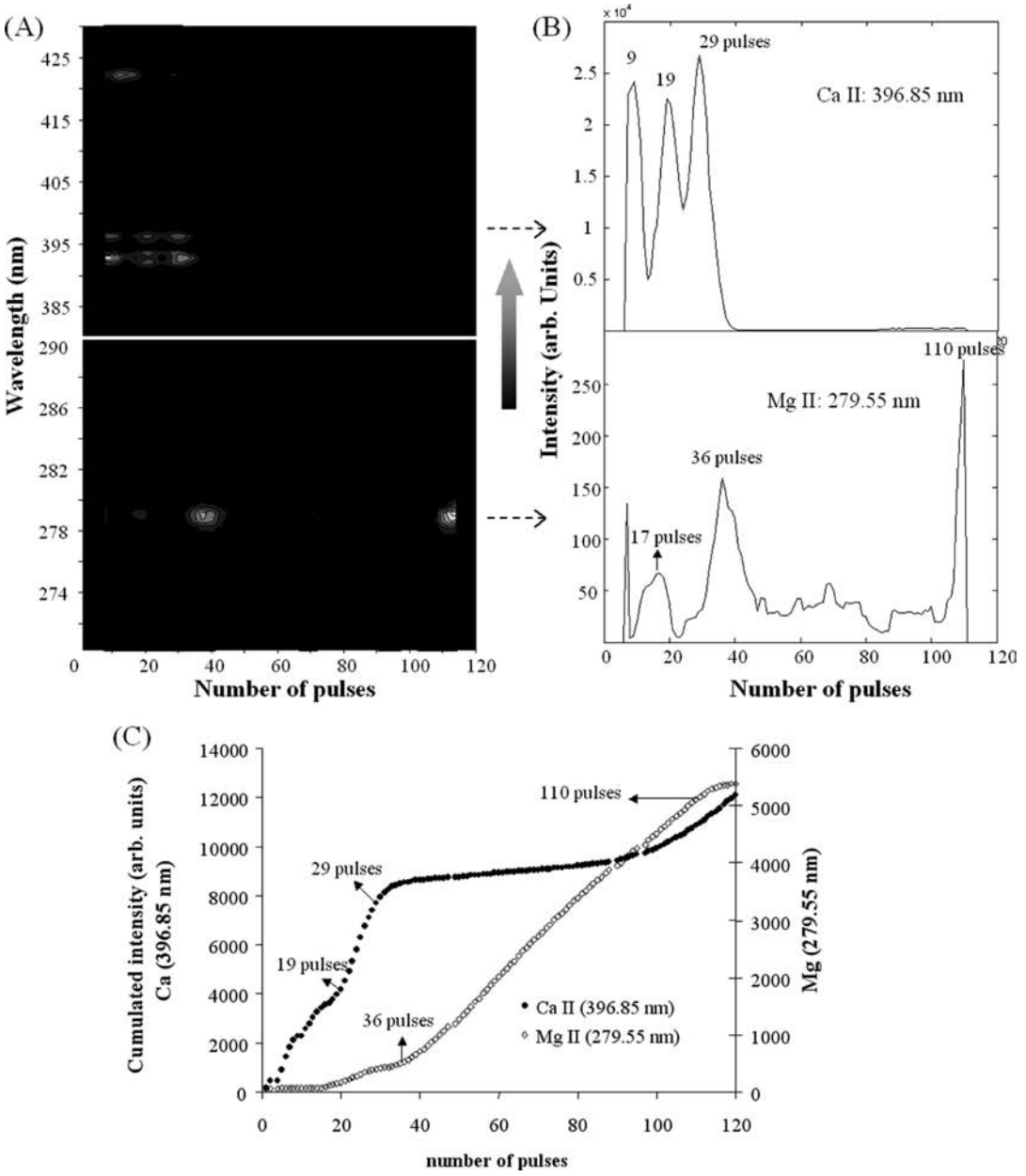

Figure 3. Exploratory analysis of LIBS spectra: (**A**) typical moving-window two-dimensional correlation spectra, (**B**) the spectral intensity transition of 2D correlation spectrum, and (**C**) the cumulated intensities at 396.85 (Ca II) and 279.55 nm (Mg II) calculated from baseline corrected and normalized spectra during wheat ablation from 1 to 120 pulses.

NE cuticule were still present (**Figure 4C**). The ablation of AL was observed after 38 pulses (**Figure 4D**). Therefore, SC and AL ablation were observed during the Ca II and Mg II intensity increase, respectively. Hence, MW2D and univariate analysis might discriminate SC and AL tissues. Because they are located between the other tissues, PE, NE, and the starchy endosperm (END) could be also discriminated. However, the position of the transition between two tissues was not possible to determine precisely. The challenge was then to be able to identify the number of pulses to ablate each tissue or even to know the spectral variables (wavelength) that can be correlated with chemical differences between the tissues by spectral data multivariate analysis considering the entire spectral range (200−1200 nm).

Supervised Multivariate Classification. The PLS-DA was generated using five classes of tissues: PE, SC, NE, AL, and END. The spectral data were normalized according to the intensity of the C_2 Swan Molecular Band (516.52 nm). Spectral data used in the calibration data set were chosen based on Ca II and Mg II intensities as described previously: only a few spectra in the middle of each tissue ablation were selected. There were 255 spectra included in the calibration data set, coming from 12 to 13 grains for each cultivar (Crousty and Tiger were used, and 3−4 spectra per class and per grain). Spectral range varied from 230 to 930 nm, avoiding some regions that could be out of the limit of spectrometer intensity (4000 au) according to the layer (390−403, 593−700, 740−790 nm). The discrimination performance was evaluated by cross-validation and by samples in an external validation data set (81 spectra). The optimal number of LVs was first evaluated by root-mean-square errors of calibration (RMSEC) using the internal cross-validation and root-mean-square errors of prediction (RMSEP) using a test data set (**Figure 5A**). Both errors had a decreasing tendency as the number of LVs increased. No increase of RMSEP for the highest LV was observed, suggesting no overfitting. This model feature has been

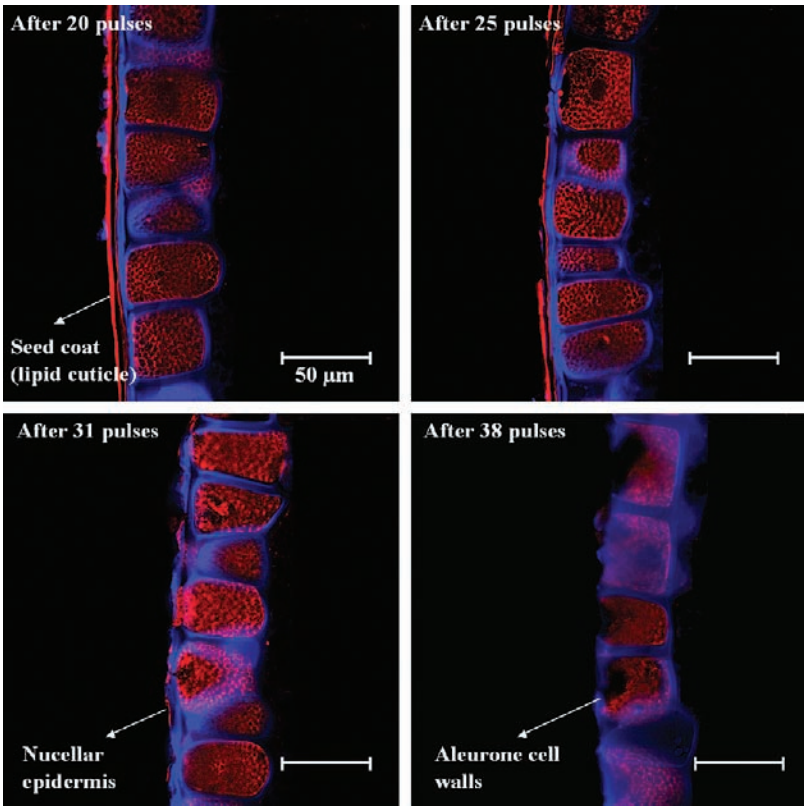

Figure 4. Cross-sections of target grains ablated up to spectral data modification given by univariate analysis of Ca II (396.85 nm) and Mg II (279.55 nm) intensities: (**A**) the start (20 pulses), (**B**) the middle (25 pulses), (**C**) the end (31 pulses) of the Ca II intensity increase, and (**D**) the start of the Mg II intensity increase at 38 pulses, respectively, using an ArF 193 nm (1 Hz, 2 J cm^{-2}). Cross-sections of Crousty were stained with Nile Red and Calcofluor and observed using CSLM.

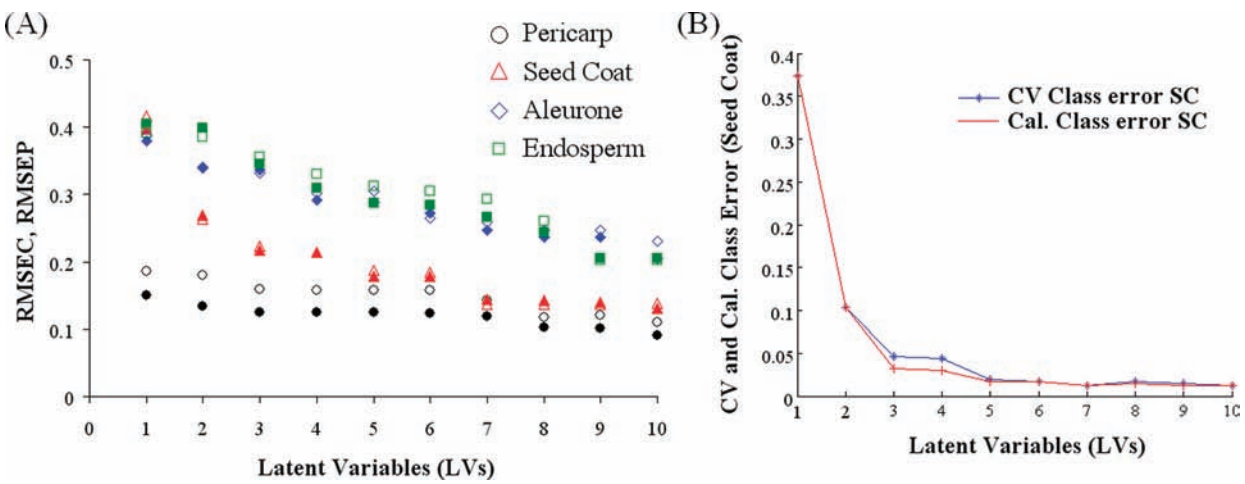

Figure 5. Discrimination performance of the PLS-DA method in function of the number of latent variables (LVs) using a cross-validation or an external validation: (**A**) root-mean-square errors of calibration (RMSEC, solid shapes) and root-mean-square errors of prediction (RMSEP, empty shapes) for four tissue classes: pericarp, seed coat, aleurone, and endosperm, and (**B**) the cross-validation (CV) or calibration (Cal) classification errors for the seed coat (SC) class.

checked for all the tissues (data not shown). The greatest difference was observed for the SC class, RMSEC and RMSEP dropped significantly from 1 to 5 LVs, decreasing a little more from 6 to 7 LVs. For this class, the cross-validation classification error in relation to the calibration classification error indicated that at 5 LVs, the minimal error was observed (**Figure 5B**). Five latent variables were then a good compromise to obtain a model with high specificity. The first five LVs variance explained 96.7% of the total variance of the spectra. As shown in **Table 1**, the PE, SC, AL, and END classes were predicted with a high sensitivity (0.97 to 1) and specificity (0.95 to 1). As expected, a high percentage of correct classification was observed for PE, SC, AL, and END. PE spectra were predicted as another layer (double classification) in 24% of the cases. NE class was predicted with a high sensitivity (0.97) but a lower specificity (0.54), indicating a limited efficacy and efficiency for NE prediction. This tissue was ablated with less than four pulses, limiting the choice of NE spectra for the calibration set. Moreover, mixed signature could

Table 1. Classification of Wheat Grain Peripheral Tissues Using PLS-DA Method (Partial Least Squares−Discriminant Analysis) from LIBS Spectra (5 Latent Variables)

	calibration			validation		
wheat tissues	no. of spectral data	sensitivity	specificity	no. of spectral data	% correct classification	% noncorrect or double classification
pericarp	52	1.000	1.000	17	100	24
seed coat	50	1.000	0.966	18	100	0
nucellar epidermis	33	0.970	0.536	11	0	36
aleurone	50	1.000	0.995	17	100	0
endosperm	70	0.986	0.946	18	100	0

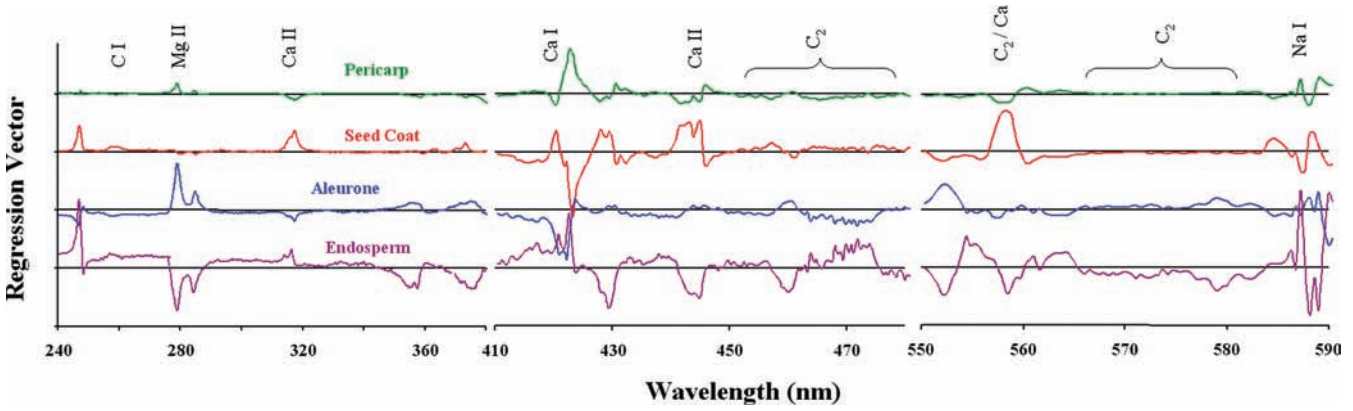

Figure 6. Regression vectors obtained by the PLS-DA to predict wheat tissues: pericarp (PE), seed coat (SC), aleurone layer (AL), and endosperm (END).

be easily obtained with adjacent tissue (SC and AL). The PLS-DA (Crousty and Tiger cultivars) could then predict and discriminate PE, SC, AL, and END. OP and IP were not distinguished, and NE was not predicted.

The PLS-DA regression vector provided information about spectral region used to discriminate tissues. The regression vectors are shown in **Figure 6**. Magnesium (Mg I, 285.22 nm; Mg II, 279.55 nm) clearly contributed to the discrimination of the SC and AL tissues. SC was also differentiated by the presence of calcium (Ca II, 315.89; 445.48 nm). END presented a smaller contribution of calcium. These results are in agreement with the main elemental differences encountered on wheat outer tissue composition (*34*).

The next step was to use the PLS-DA to predict all LIBS spectra and then follow the wheat grain ablation. During ablation, PE was identified first, then SC, AL, and finally END, in agreement with the anatomical structure of the wheat grain. In the case of the sample shown in **Figure 3C**, the PE ablation was predicted from 3 to 13 pulses, then the SC, from 19 to 30 pulses, the AL, from 37 to 101 pulses, and finally, the END ablation, after 111 pulses. No double predictions were observed in this case, but some LIBS spectra were not classified during tissue transition, mainly between PE and SC (about 6 ± 1 pulses). This could be due to gradual ablation of the thin wheat tissues ($< 70\ \mu$m) and the possible heterogeneous laser spot, inducing mixed information from both adjacent tissues. These prediction problems could underestimate the number of pulses to ablate the PE, SC, AL, and END.

The number of pulses to ablate each tissue is shown in **Table 2**. Results showed that PE from Tiger seems to be more difficult to be ablated (21 ± 4 pulses) than PE from Crousty (17 ± 3 pulses), however tissue thickness needs to be measured in order to avoid erroneous interpretation. The number of pulses predicted by the PLS-DA method are similar to those observed by microscopic observations in a previous work (*10*).

Wheat Tissue Ablation Rate by LIBS. Because the outer tissue can have different thickness, the ablation rates calculated were required in order to compare the behavior of the wheat cultivars.

Table 2. Ablation Rate, *Ar* (μm/Pulse) for Different Wheat Tissues[a]

	thickness (μm)		ΔNp (pulse)		*Ar* (μm/pulse)	
	Crousty	Tiger	Crousty	Tiger	Crousty	Tiger
pericarp	56 ± 8	63 ± 5	18 ± 3	20 ± 3	3.2 ± 0.6	3.2 ± 0.5
seed coat	4.6 ± 0.5	4.5 ± 0.3	11 ± 3	14 ± 5	0.5 ± 0.1	0.4 ± 0.1
aleurone	81 ± 5	72 ± 10	55 ± 7	56 ± 9	1.5 ± 0.2	1.3 ± 0.2

[a] Ablation rate was given by the matter ablated per number of pulses. Tissue thickness (μm) was deduced from image analysis of nonablated samples, and the number of pulses (ΔNp) was given by PLS-DA prediction obtained from spectra acquired during the ablation of 12−13 wheat grains/cultivar.

Tissue ablation rate (*Ar*, μm/pulse) was defined as the amount of material loss per pulse (*Np*). PE and AL ablation rates were given according to eq 2 and seed coat according to eq 3.

$$Ar(\text{PE or AL}) = \frac{\overline{Wt}}{\Delta Np} \tag{2}$$

$$Ar(\text{SC}) = \frac{\overline{St}}{\Delta Np} \times \frac{1}{184.3\mu\text{m}} \tag{3}$$

where $\overline{Wt}$ (μm) and $\overline{St}$ (μm^2) are the average of the object width and surface of the tissue given by microscopic image analysis of nonablated samples, respectively. These values were taken from a previous work (*10*). PE and AL were considered as a rectangular tissue, and so their thicknesses were compared to the object width, and SC thickness was given by its object surface divided by the image dimension (184.3 μm) in order to obtain the equivalent tissue thickness. The number of pulses was predicted for each grain, which presented a value of *Ar* for each tissue (**Table 2**).

The SC was the most difficult tissue to be ablated and the PE the least difficult, regardless of the cultivars. Considering that wheat outer tissues were ablated in the same conditions, differences between each tissue ablation rate could be related to their mechanical properties (*40*). Thus, the SC presented the lower ablation rate for both cultivars, suggesting that this was the most cohesive tissue of wheat outer tissues.

This study showed a first attempt to apply chemometric pattern recognition procedure in the context of classification and discrimination of vegetal materials using LIBS data. An unsupervised method, the MW2D correlation, was useful to reveal spectral transitions during the wheat outer tissues ablation. These spectral transitions corresponded to the anatomical transitions as confirmed by microscopy of the cross-sections of target grains. The use of MW2D correlation and the traditional univariate analysis of target emission lines based on tissue compositional differences allowed having spectral data references from each tissue. The use of PLS-DA, a supervised pattern recognition technique, was then successfully applied to discriminate wheat tissues (PE, SC, AL, and END) and predict the number of pulses to ablate them. Thus, the ablation rate (material loss/pulse) was calculated for each predicted tissue with the aid of microscopy, and these results were related to the tissue cohesion. The possibility to compare the ablation rate to the tissue cohesion could be a potential technique to investigate physicochemical bases of wheat tissues in situ directly on the native grain. Therefore, LIBS experiments used in conjunction with multivariate analysis could be an interesting technique for rapid structural analysis of vegetal material.

ABBREVIATIONS USED

LIBS, laser-induced breakdown spectroscopy; PLS-DA, partial least squares−discriminant analysis; MW2D, moving-window two-dimensional correlation; PCA, principal component analysis; LV(s), latent variable(s); OP, outer pericarp; IP, inner pericarp; PE, pericarp (outer + inner); SC, seed coat; NE, nucellar epidermis; AL, aleurone layer; END, starchy endosperm; CSLM, confocal scanning laser microscopy; *Ar*, tissue ablation rate (μm/pulse); *Np*, number of pulses; $\overline{Wt}$, average of the object width of the tissue given by microscopic image analysis of nonablated samples (μm); $\overline{St}$, average of the object surface of the tissue given by microscopic image analysis of non ablated samples (μm^2).

ACKNOWLEDGMENT

We express our gratitude to the Montpellier RIO imaging (MRI) microscopy facility.

LITERATURE CITED

(1) Bradbury, D.; McMasters, M. M.; Cull, I. M. Structure of the wheat kernel. II. Microscopic structure of pericarp, seed coat, and other coverings of the endosperm and germ of hard red winter wheat. *Cereal Chem*. **1956**, *33*, 342–360.

(2) Pomeranz, Y. Chemical composition of kernel structures. In *Wheat: Chemistry and Technology*; Pomeranz, Y., Ed.; AACC: St Paul, MN, 1988; Vol. 4, pp 97−158.

(3) Greffeuille, V.; Abecassis, J.; Lapierre, C.; Lullien-Pellerin, V. Bran size distribution at milling and mechanical and biochemical characterization of common wheat grain outer layers: a relationship assessment. *Cereal Chem*. **2006**, *83*, 641–646.

(4) Peyron, S.; Chaurand, M.; Rouau, X.; Abecassis, J. Relationship between bran mechanical properties and milling behaviour of durum wheat (*Triticum durum* Desf.). Influence of tissue thickness and cell wall structure. *J. Cereal Sci*. **2002**, *36*, 377–386.

(5) Antoine, C.; Peyron, S.; Mabille, F.; Lapierre, C.; Bouchet, B.; Abecassis, J.; Rouau, X. Individual contribution of grain outer layers and their cell wall structure to the mechanical properties of wheat bran. *J. Agric. Food Chem*. **2003**, *51*, 2026–2033.

(6) Glenn, G. M.; Johnston, R. K. Moisture-dependent changes in mechanical properties of isolated wheat bran. *J. Cereal Sci*. **1992**, *15*, 223–236.

(7) Greffeuille, V.; Mabille, F.; Rousset, M.; Oury, F. X.; Abecassis, J.; Lullien-Pellerin, V. Mechanical properties of outer layers from near-isogenic lines of common wheat differing in hardness. *J. Cereal Sci*. **2007**, *45*, 227–235.

(8) Peyron, S.; Abecassis, J.; Autran, J. C.; Rouau, X. Enzymatic oxidative treatments of wheat bran layers: effects on ferulic acid composition and mechanical properties. *J. Agric. Food Chem*. **2001**, *49*, 4694–4699.

(9) Barron, C.; Surget, A.; Rouau, X. Relative amounts of tissues in mature wheat (*Triticum aestivum* L.) grain and their carbohydrate and phenolic acid composition. *J. Cereal Sci*. **2007**, *45*, 88–96.

(10) Martelli, M. R.; Barron, C.; Delaporte, P.; Viennois, G.; Rouau, X.; Sadoudi, A. Pulsed laser ablation: a new approach to reveal wheat outer layer properties. *J. Cereal Sci*. **2009**, *49*, 354–362.

(11) Hola, M.; Otruba, V.; Kanicky, V. Influence of binders on infrared laser ablation of powdered tungsten carbide pressed pellets in comparison with sintered tungsten carbide hard metals studied by inductively coupled plasma atomic emission spectrometry. *Spectrochim. Acta, Part B* **2006**, *61*, 515–524.

(12) Larkin, R. A.; McMaster, T. C.; Wolf, M. J.; Rist, C. E. Studies on the relation of bran thickness to millability of some Pacific Northwest wheats. *Cereal Chem*. **1951**, *28*, 247–258.

(13) Crewe, J.; Jones, C. R. The thickness of wheat bran. *Cereal Chem*. **1951**, *28*, 40–49.

(14) Hussain, T.; Gondal, M. A.; Yamani, Z. H.; Baig, M. A. Measurement of nutrients in green house soil with laser induced breakdown spectroscopy. *Environ. Monit. Assess*. **2007**, *124*, 131–139.

(15) Baudelet, M.; Boueri, M.; Yu, J.; Mao, S. S.; Piseltelli, V.; Mao, X. L.; Russo, R. E. Time-resolved ultraviolet laser-induced breakdown spectroscopy for organic material analysis. *Spectrochim. Acta, Part B* **2007**, *62*, 1329–1334.

(16) Labbe, N.; Swamidoss, I. M.; Andre, N.; Martin, M. Z.; Young, T. M.; Rials, T. G. Extraction of information from laser-induced breakdown spectroscopy spectral data by multivariate analysis. *Appl. Opt*. **2008**, *47*, G158–G165.

(17) Portnov, A.; Rosenwaks, S.; Bar, I. Identification of organic compounds in ambient air via characteristic emission following laser ablation. *J. Lumin*. **2003**, *102*, 408–413.

(18) Xu, H. L.; Mejean, G.; Liu, W.; Kamali, Y.; Daigle, J. F.; Azarm, A.; Simard, P. T.; Mathieu, P.; Roy, G.; Simard, J. R.; Chin, S. L. Remote detection of similar biological materials using femtosecond filament-induced breakdown spectroscopy. *Appl. Phys. B: Lasers Opt*. **2007**, *87*, 151–156.

(19) St-Onge, L.; Sing, R.; Bechard, S.; Sabsabi, M. Carbon emissions following 1.064 mu m laser ablation of graphite and organic samples in ambient air. *Appl. Phys. A: Mater*. **1999**, *69*, S913–S916.

(20) Salle, B.; Cremers, D. A.; Maurice, S.; Wiens, R. C.; Fichet, P. Evaluation of a compact spectrograph for in situ and stand-off laser-induced breakdown spectroscopy analyses of geological samples on Mars missions. *Spectrochim. Acta, Part B* **2005**, *60*, 805–815.

(21) Trevizan, L. C.; Santos, D., Jr.; Samad, R. E.; Vieira, N. D., Jr.; Nomura, C. S.; Nunes, L. C.; Rufini, I. A.; Krug, F. J. Evaluation of laser induced breakdown spectroscopy for the determination of macronutrients in plant materials. *Spectrochim. Acta, Part B* **2008**, *63*, 1151–1158.

(22) Trevizan, L. C.; Santos, D., Jr.; Samad, R. E.; Vieira, N. D., Jr.; Nunes, L. C.; Rufini, I. A.; Krug, F. J. Evaluation of laser induced breakdown spectroscopy for the determination of micronutrients in plant materials. *Spectrochim. Acta, Part B* **2009**, *64*, 369–377.

(23) Galiova, M.; Kaiser, J.; Novotny, K.; Novotny, J.; Vaculovic, T.; Liska, M.; Malina, R.; Stejskal, K.; Adam, V.; Kizek, R. Investigation of heavy-metal accumulation in selected plant samples using laser induced breakdown spectroscopy and laser ablation inductively coupled plasma mass spectrometry. *Appl. Phys A: Mater*. **2008**, *93*, 917–922.

(24) Galiova, M.; Kaiser, J.; Novotny, K.; Samek, O.; Reale, L.; Malina, R.; Palenikova, K.; Liska, M.; Cudek, V.; Kanicky, V.; Otruba, V.; Poma, A.; Tucci, A. Utilization of laser induced breakdown spectroscopy for investigation of the metal accumulation in vegetal tissues. *Spectrochim. Acta, Part B* **2007**, *62*, 1597–1605.

(25) Hybl, J. D.; Lithgow, G. A.; Buckley, S. G. Laser-induced breakdown spectroscopy detection and classification of biological aerosols. *Appl. Spectrosc*. **2003**, *57*, 1207–1215.

(26) Jurado-Lopez, A.; de Castro, M. D. L. Chemometric approach to laser-induced breakdown analysis of gold alloys. *Appl. Spectrosc*. **2003**, *57*, 349–352.

(27) Martin, M. Z.; Labbe, N.; Rials, T. G.; Wullschleger, S. D. Analysis of preservative-treated wood by multivariate analysis of laser-induced breakdown spectroscopy spectra. *Spectrochim. Acta, Part B* **2005**, *60*, 1179–1185.
(28) Laville, S.; Sabsabi, M.; Doucet, F. R. Multi-elemental analysis of solidified mineral melt samples by laser-induced breakdown spectroscopy coupled with a linear multivariate calibration. *Spectrochim. Acta, Part B* **2007**, *62*, 1557–1566.
(29) Doucet, F. R.; Faustino, P. J.; Sabsabi, M.; Lyon, R. C. Quantitative molecular analysis with molecular bands emission using laser-induced breakdown spectroscopy and chemometrics. *J. Anal. Atom. Spectrom.* **2008**, *23*, 694–701.
(30) Geladi, P. Chemometrics in spectroscopy. Part 1. Classical chemometrics. *Spectrochim. Acta, Part B* **2003**, *58*, 767–782.
(31) Geladi, P.; Sethson, B.; Nystrom, J.; Lillhonga, T.; Lestander, T.; Burger, J. Chemometrics in spectroscopy, Part 2. Examples. *Spectrochim. Acta, Part B* **2004**, *59*, 1347–1357.
(32) Barker, M.; Rayens, W. Partial least squares for discrimination. *J. Chemom.* **2003**, *17*, 166–173.
(33) Thomas, M.; Richardson, H. H. Two-dimensional FT-IR correlation analysis of the phase transitions in a liquid crystal, 4′-*n*-octyl-4-cyanobiphenyl (8CB). *Vib. Spectrosc.* **2000**, *24*, 137–146.
(34) Heard, P. J.; Feeney, K. A.; Allen, G. C.; Shewry, P. R. Determination of the elemental composition of mature wheat grain using a modified secondary ion mass spectrometer (SIMS). *Plant J.* **2002**, *30*, 237–245.
(35) *2D-Shige*, http://sci-tech.ksc.kwansei.ac.jp/∼ozaki/2D-shige.htm (accessed in September 2009).
(36) Parkkonen, T.; Heinonen, R.; Autio, K. A new method for determining the area of cell walls in rye doughs based on fluorescence microscopy and computer-assisted image analysis. *Lebensm. Wiss. Technol.* **1997**, *30*, 743–747.
(37) *NIST Atomic Spectra Database*, http://physics.nist.gov/PhysRefData/ASD/lines_form.html (accessed in September 2009).
(38) Evers, A. D.; Bechtel, D. B. Microscopic structure of the wheat grain. In *Wheat: Chemistry and Technoloy*; Pomeranz, Y., Ed.; AACC: St Paul, MN, 1988; Vol. 1, pp 47−95.
(39) Barron, C.; Rouau, X. FTIR and Raman signatures of wheat grain peripheral tissues. *Cereal Chem.* **2008**, *85*, 619–625.
(40) Walsh, J. T.; Deutsch, T. F. Pulsed CO_2 laser ablation of tissue: effect of mechanical properties. *IEEE Trans. Bio-Med. Eng.* **1989**, *36*, 1195–201.

Received for review February 17, 2010. Revised manuscript received May 3, 2010. Accepted May 14, 2010. This study is financially supported by the European Commission in the Communities sixth Framework Programme, Project HEALTHGRAIN (FP6-514008). This publication reflects only the authors' views and the Community is not liable for any use that may be made of the information contained in this article.